

Resilient Channel Charting Under Varying Radio Link Availability

Jonas Pirk¹, Jonathan Ott¹, Maximilian Stahlke¹, George Yammine¹, Tobias Feigl^{1,2}, and Christopher Mutschler¹

{jonas.pirk, jonathan.ott, maximilian.stahlke, tobias.feigl, christopher.mutschler}@iis.fraunhofer.de

¹ Fraunhofer Institute for Integrated Circuits (IIS), Division Positioning and Networks, 90411 Nürnberg, Germany

² Computer Science Department, Friedrich-Alexander-Universität Erlangen-Nürnberg, 91052 Erlangen, Germany

Abstract—Channel charting (CC) has become a key technology for RF-based localization, enabling unsupervised radio fingerprinting, even in non line of sight scenarios, with a minimum of reference position labels. However, most CC models assume fixed-size inputs, such as a constant number of antennas or channel measurements. In practical systems, antennas may fail, signals may be blocked, or antenna sets may change during handovers, making fixed-input architectures fragile. Existing radio-fingerprinting approaches address this by training separate models for each antenna configuration, but the resulting training effort scales prohibitively with the array size.

We propose Adaptive Positioning (AdaPos), a CC architecture that natively handles variable numbers of channel measurements. AdaPos combines convolutional feature extraction with a transformer-based encoder using learnable antenna identifiers and self-attention to fuse arbitrary subsets of CSI inputs. Experiments on two public real-world datasets (SISO and MIMO) show that AdaPos maintains state-of-the-art accuracy under missing-antenna conditions and replaces roughly 57 configuration-specific models with a single unified model. With AdaPos and our novel training strategies, we provide resilience to both individual antenna failures and full-array outages.

I. INTRODUCTION

RF-based positioning becomes increasingly important for applications such as smart factories, traffic hotspot identification, and emergency services [1]. Traditional localization methods, such as time-difference of arrival (TDoA), require line-of-sight (LOS) signals and degrade in the presence of multipath propagation [2]. In indoor environments, where non-line-of-sight (NLOS) conditions and signal blockages occur frequently, these methods often fail to provide reliable accuracy [2]. Radio fingerprinting offers an alternative by mapping measured radio features to positions and has shown promising performance in indoor scenarios [2]. However, fingerprinting depends on large labeled datasets, and collecting such data remains time-consuming and expensive [2].

CC addresses this limitation by learning a low-dimensional representation of channel state information (CSI) that reflects the spatial neighborhood structure without requiring reference location labels [3], [4], [5], [6]. CC maps the CSI manifold to a latent space using pseudo-distance metrics, enabling scalable, unsupervised RF localization [3]. Most fingerprinting [7] and CC approaches [5], [8] assume a fixed input size, meaning that the number of antennas or channel measurements remains

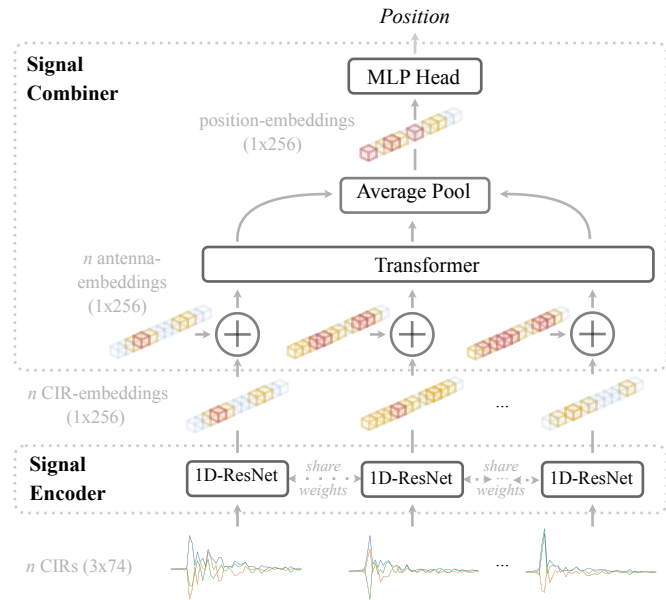


Fig. 1. Overview of the AdaPos architecture. Information flows from bottom to top. We first pass individual channel impulse responses (CIRs) through a signal encoder (1D-ResNet) that creates one embedding per CIR. Next, the signal combiner adds an antenna embedding to each CIR embedding so the model identifies the source antenna. A transformer encoder then combines the set of CIR embeddings through self-attention. Its output is average-pooled and passed through an MLP head to return the CC pseudo 2D positions.

constant. In practice, however, antenna availability changes: antennas may be powered down to save energy [9], signals may be blocked [10], or hardware failures may occur [11]. These situations lead to variable radio link availability, which breaks fixed-input models. Existing solutions address this by training separate models for different antenna configurations and selecting the appropriate model during inference [7]. Since the number of antenna subsets grows exponentially with the array size ($\mathcal{O}(2^n)$), training and maintaining configuration-specific models quickly becomes infeasible.

Our paper addresses these limitations. We propose AdaPos (see Fig. 1), a CC architecture that handles a variable numbers of channel measurements natively. AdaPos uses a shared Convolutional Neural Network (CNN) to extract CIR em-

beddings, augments them with learnable antenna identifiers, and employs a transformer-based encoder to fuse arbitrary subsets of CIRs through self-attention [12]. This allows a single model to adapt to changing antenna configurations without retraining. We further introduce training strategies that simulate antenna dropouts and improve robustness when only few signals are available. These strategies also allow existing models to handle missing antennas without architecture changes. In this way, AdaPos avoids the exponential growth of configuration-specific models and provides a scalable solution for large antenna arrays. We evaluate AdaPos on two real-world datasets ($B_1 = 50\text{ MHz}$, $f_{c1} = 1.3\text{ GHz}$ and $B_2 = 100\text{ MHz}$, $f_{c2} = 3.7\text{ GHz}$) and test a range of missing-antenna scenarios. The experiments show that AdaPos maintains state-of-the-art performance (maximum of 6 cm deviation) across varying antenna configurations and replaces roughly 57 configuration-specific models with one unified model while keeping nearly unchanged error performance.

The remainder of this paper is organized as follows. Sec. II discusses related work. Sec. III describes the AdaPos architecture and training strategies. Sec. IV presents the datasets and evaluation setup, and Sec. V reports the experimental results, before Sec. VI concludes.

II. RELATED WORK

CC was introduced as a scalable alternative that removes the dependence on labeled reference positions. CC learns a lower-dimensional representation of CSI that preserves the spatial neighborhood structure of the high-dimensional space [3].

Early work uses classical dimensionality-reduction methods such as PCA [3], Sammons Mapping [3], autoencoders [3] or t-SNE [13]. More recently, neural-network-based methods use pseudo-distance metrics, that CC uses to map high-dimensional CSI to a lower-dimensional latent space, enabling unsupervised localization. These pseudo-distances can be derived directly from CSI [14], [15] or from auxiliary modalities such as timestamps [5] or pedestrian dead reckoning (PDR) [4]. Recent metrics explore using geodesic distances [15] or fusing multiple metrics [6] to improve quality of the resulting channel chart.

Popular architectures are based on neural networks and include, for instance, Siamese networks [6], [8], [16], [17] and triplet networks [5]. Triplet networks [18] optimize a contrastive objective, where samples close in the data space are pulled together in the latent space, while distant samples are pushed apart. In CC, temporal proximity can serve as a proxy for spatial proximity: samples recorded within short intervals are assumed to be close in distance, while samples separated by longer intervals are expected to be farther apart because the person has moved more [5]. Siamese networks [19] are trained to predict positions by minimizing the mismatch between the Euclidean distance of two predicted positions and the pseudo-distance between the corresponding samples [16]. These parametric models are efficient at inference and can learn complex CSI-distance relationships.

However, neural network (NN)-based CC methods typically assume the same antennas are available at training and inference [6], [8], [15]. When antenna availability changes, these models degrade or fail. A common workaround is to train a separate model for each antenna subset and select the appropriate model during inference [7]. While feasible in small systems, this approach does not scale. The number of possible antenna subsets grows exponentially ($\mathcal{O}(2^n)$), making it impractical for arrays with many elements.

In contrast to existing approaches, we provide a single model, that handles any antenna configuration natively. By designing a model that processes variable numbers of CIRs and remains robust to missing antennas, we remove the need for configuration-specific models and address the scalability challenges inherent in existing CC and fingerprinting solutions.

III. METHOD

We first introduce the AdaPos architecture and then explain how we train and handle varying antenna availability in CC.

A. Network Architecture

To accommodate variable numbers of received signals, i.e. radio links, we propose our flexible transformer-based model called AdaPos. The architecture consists of two main components: a signal encoder and a signal combiner, see Fig. 1.

The **Signal Encoder** (lower part in Fig. 1) processes individual CIRs and creates a compact embedding that captures their most relevant features. It is implemented as a lightweight 1D-ResNet whose weights are shared across all CIR inputs, which reduces the number of parameters and improves generalization. The resulting embeddings are passed directly to the signal combiner.

The **Signal Combiner** (upper part in Fig. 1) fuses an arbitrary set of embeddings and predicts the final position. It supports any number of inputs and learns how much each contributes to the final estimate. Its core mechanism is a self-attention layer [12], which dynamically extracts relevant information from all available embeddings. For each input embedding, the attention module forms a weighted sum of all embeddings, where the weights are derived from learned similarity scores. As the weighted sum has a fixed output size independent of the number of inputs, the model naturally handles varying antenna counts. However, this operation is permutation-invariant. To retain information about the origin of each CIR, we add a learnable antenna-specific embedding to each CIR embedding, allowing the model to identify the source antenna. This approach improves performance under dynamic antenna availability as the attention weights depend directly on the available inputs, in contrast to CNNs or multi-layer perceptrons (MLPs), which rely on fixed receptive fields or fixed input dimensions. We implement the signal combiner as a compact transformer encoder [12] with a hidden dimensionality of 256, 8 attention heads, and a feed-forward layer of size 1024, using a total of 3 encoder layers. The transformer output is average-pooled and passed through an MLP head to predict the 2D position.

B. Model Training

We adopt a Siamese training strategy to project high-dimensional CSI into a 2D coordinate space. 2 samples pass through the same network, and the loss enforces that the Euclidean distance between the predicted positions matches the pseudo-distance derived from the CC metric. The loss function is defined as

$$\mathcal{L}_\theta(x_n, x_k, d_{n,k}) = (d_{n,k} - \|f_\theta(x_n) - f_\theta(x_k)\|_2)^2, \quad (1)$$

where f_θ denotes the neural network with parameters θ , x_n and x_k are two CIR samples, and $d_{n,k}$ their pseudo-distance.

IV. EXPERIMENTAL SETUP

We first introduce the training strategies employed for AdaPos and the ResNet baseline. Next, we summarize the datasets and preprocessing steps, followed by the training configuration used in all experiments.

A. Training Strategies

We investigate two training strategies for both AdaPos and a ResNet baseline architecture: (1) Fixed-N and (2) Random-N. Fixed-N trains the models with a fixed number of antennas n_t , ranging from 1 to a_{\max} , where a_{\max} is the maximum number of antennas available in the dataset. In each batch, we select n_t random antennas and pass them through the model. Random-N first samples the number of antennas n_t uniformly for every batch ($n_t \sim \mathcal{U}(1, a_{\max})$), and then select n_t random antennas as inputs. In general, for optimization, we use an AdamW optimizer [20] and apply a linear warmup schedule [12] for the learning rate to stabilize training during the initial epochs, and a weighted mean squared error (MSE) loss, Sec. III-A.

B. Dataset

To evaluate the proposed approach, we use 2 real-world datasets: the Dichasus dataset [21] and the Fraunhofer 5G dataset [22]. These datasets represent diverse environments and antenna configurations, providing a robust basis for evaluating model robustness under varying antenna availability.

Dichasus Dataset [21] covers a MIMO setup recorded in an industrial environment using four antenna arrays, each consisting of eight antenna elements. The system uses a 50.056 MHz bandwidth at a center frequency of 1.272 GHz. The dataset provides CSI sampled at 20.83 Hz, which we transform into the time domain and normalize to the range [0, 1]. Each CIR has a resolution of 80 samples and 3 channels: real part, imaginary part, and the absolute value, similar to [23]. We employ the current state-of-the-art (SOTA) for antenna arrays as a distance metric, which is a geodesic fusion of a time-based and angle-delay profile (ADP)-based metric [6]. We train on 60,507 samples of dichasus-cf02 and dichasus-cf04, and test on 23,478 samples of dichasus-cf03.

Fraunhofer 5G Dataset covers a SISO setup recorded in a simulated industrial warehouse environment using a 5G downlink system with six receiving antennas. The radio operates at 3.7 GHz with a bandwidth of 100 MHz and a transmit power of 20 dBm. Data is recorded over an area of approximately

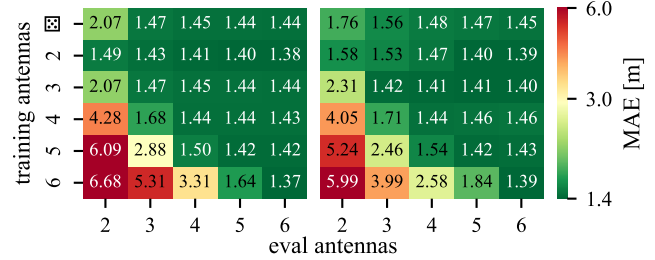


Fig. 2. MAE of ResNet (left), AdaPos (right) on the Fraunhofer 5G dataset.

400 m² at 6.6 Hz. The training set contains 18,706 samples and the test set contains 15,722 samples. This time we employ the CIRA metric [15], which also works with single antennas.

C. Training Configuration

We train and evaluate the models under various antenna configurations to assess robustness to missing antennas. Specifically, we train models for every training strategy as described in Section IV-A. We then evaluate each of the models for every possible count of antennas for the corresponding dataset. We include a ResNet-based architecture [8] as a baseline to compare how the training strategies affect transformer- and CNN-based models. For the ResNet baseline, missing antennas are handled by zeroing out the corresponding input channels. In contrast, AdaPos is designed to process variable-sized inputs directly. The learnable antenna embeddings allow the model to identify the source antenna for each CIR, so missing antennas are simply omitted from the input set.

V. EVALUATION

Benchmarking all antenna combinations is computationally infeasible. Thus, for each evaluation antenna count n_e , we randomly select the missing antennas in every batch to obtain a representative estimate of the overall performance. For a fair comparison, we use the same random antenna selections for all methods. We omit the case $n_e = 1$, as neither training nor evaluating single-antenna signals yields meaningful results due to the lack of spatial diversity, and AdaPos relies on attention weights that compare multiple embeddings, that are undefined for a single input. To compute the localization error, we apply the optimal affine transformation to map the channel chart from pseudo-coordinates to real-world coordinates.

TABLE I
BASELINE RESULTS, AVERAGED ACROSS ALL ANTENNA COMBINATIONS WITH THE SAME NUMBER OF VISIBLE ANTENNAS.

No. antennas	No. models	MAE [m]
2	15	1.43
3	20	1.39
4	15	1.39
5	6	1.39
6	1	1.37

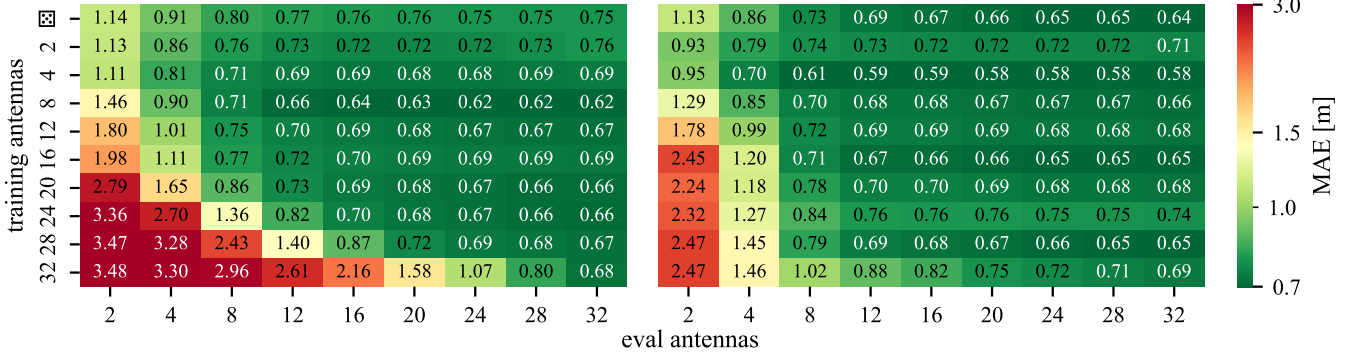


Fig. 3. MAE of ResNet (left), AdaPos (right) on the Dichasus dataset, w. single antennas masked.

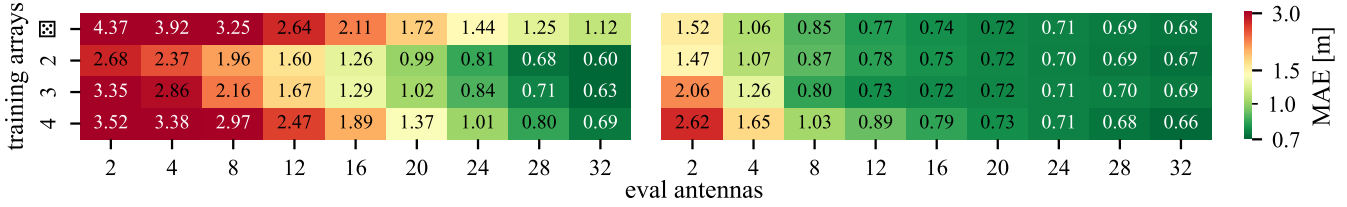


Fig. 4. ResNet (left), AdaPos (right) trained with full arrays masked and evaluated with single elements missing.

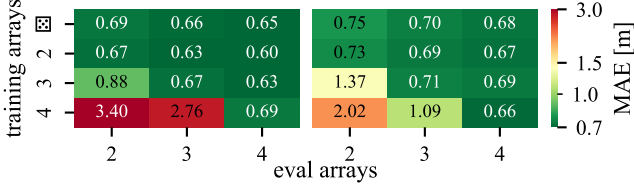


Fig. 5. MAE of ResNet (left), AdaPos (right) on the Dichasus dataset, w. arrays masked.

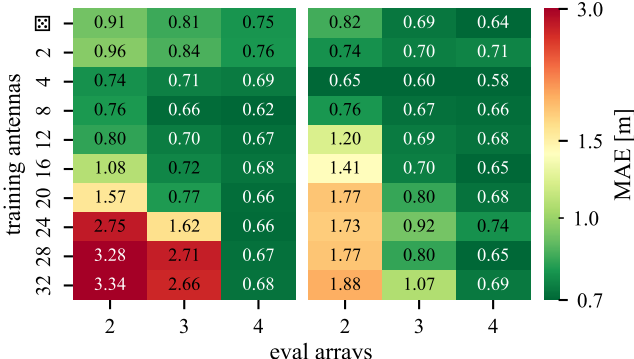


Fig. 6. ResNet (left), AdaPos (right) trained with single elements masked and evaluated with full arrays missing.

A. Evaluation on the Fraunhofer 5G Dataset

As a baseline, we train 57 configuration-specific models, one for every antenna subset containing 2 to 6 antennas.

Table I shows that performance does not vary significantly across different antenna combinations. This indicates that the accuracy is mainly limited by the CC metric rather than by the number of available antennas. Fig. 2 compares the ResNet and AdaPos models. The plots show the MAE for different pairs of (n_t, n_e) , where n_t is the number of antennas during training and n_e is the number available during inference. We also evaluate the Random-N strategy ($n_t \sim \mathcal{U}(1, a_{\max})$),

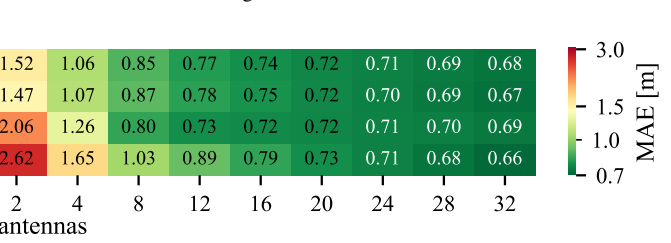
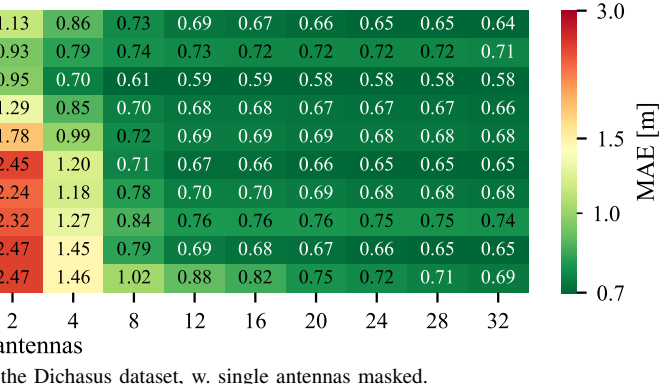


Fig. 4. ResNet (left), AdaPos (right) trained with full arrays masked and evaluated with single elements missing.

see the dice symbol in Fig. 2. As expected, reducing the number of inference antennas (n_e) generally decreases positioning accuracy. However, increasing the variability during training, i.e., reducing n_t , substantially improves robustness. For example, with only 2 antennas available at inference time, the MAE improves by up to 78% (down to 1.49 m) when training with $n_t = 2$. In certain settings, the ResNet baseline yields a marginally lower MAE. We believe this is due to the relatively small number of antenna combinations, e.g., only 15 for $n_t = 2$, that increases the likelihood that ResNet encounters all combinations during training at every position. AdaPos achieves markedly more stable performance across mismatched (n_t, n_e) pairs. In particular, AdaPos degrades insignificantly when the number of antennas during inference is lower than during training ($n_e < n_t$).

Overall, a single AdaPos model effectively replaces all 57 configuration-specific baselines. Even in the most challenging case ($n_t = 2, n_e = 2$), MAE differs only by 6 cm. In the best case ($n_t = 2, n_e = 6$), MAE differs by only 1 cm.

B. Evaluation on the Dichasus Dataset

We evaluate two scenarios: (1) missing individual antenna elements within each array and (2) missing entire antenna arrays. As the dataset consists of 4 arrays with 8 elements each, testing all antenna combinations is infeasible. So, we treat $n_e = 32$ (or $n_e = 4$ when evaluating missing arrays) as a practical lower bound.

Single Antenna Element. We consider 2 categories of models. The first category is trained with single-element masking ($a_{\max} = 32$), see Fig. 3. The second category is trained with full-array masking ($a_{\max} = 4$), see Fig. 4. Models trained with single-element masking show trends similar to the Fraunhofer dataset: AdaPos outperforms ResNet whenever $n_e < n_t$. Also, the ResNet model struggles when only a few

antennas are available ($n_e \leq 12$), whereas AdaPos remains robust across all training strategies. Interestingly, training on 4 single-element masks ($n_t = 4$) yields the best-performing AdaPos model, reflecting that optimal training strategies are dataset-dependent. When training with entire arrays masked, the ResNet model performs poorly overall. AdaPos improves over ResNet but still falls short of the model trained with single-element masking. So, using AdaPos with single-element masking improves generalization, even when entire arrays fail.

Antenna Arrays. We evaluate the performance when whole arrays are missing, see Fig. 5. Here, the ResNet baseline performs slightly better than AdaPos in most settings except when all arrays are present ($n_e = 4$). However, when training with single-element masking rather than array masking, see Fig. 6, the best AdaPos model ($n_t = 4$) outperforms the best array-masked baseline (ResNet with $n_t = 2$). So, training with single-element masking yields a model that is robust not only to isolated antenna failures but also to complete array outages.

VI. CONCLUSION

We presented AdaPos, a transformer-based CC architecture that natively handles variable radio link availability. Our approach eliminates the need for exponentially many configuration-specific models, an otherwise intractable requirement for large arrays, while maintaining SOTA localization accuracy. Experiments on 2 real-world datasets show that a single AdaPos model replaces a large number of configuration-specific baselines. On SISO 5G CSI, we substituted 57 dedicated models with only a marginal accuracy loss (at most 6 cm MAE) and consistently generalizes better across mismatched training-inference antenna configurations. On MIMO CSI, AdaPos trained with single-element masking provides strong resilience against both individual element failures and full-array outages, outperforming models trained solely on array masking. The optimal masking strategy is dataset-dependent, but the Random-N strategy yields robust performance without per-dataset tuning.

VII. ACKNOWLEDGMENTS

This work was supported by the Federal Ministry of Education and Research of Germany in the programme of “Souverän. Digital. Vernetzt.” joint project 6G-RIC (16KISK020K).

REFERENCES

- [1] C. Laoudias, A. Moreira, S. Kim, S. Lee, L. Wirola, and C. Fischione, “A survey of enabling technologies for network localization, tracking, and navigation,” *IEEE Comms. Surveys & Tutorials*, vol. 20, no. 4, pp. 3607–3644, 2018.
- [2] D. Dardari, P. Closas, and P. M. Djurić, “Indoor tracking: Theory, methods, and technologies,” *IEEE Trans. on Vehicular Technology*, vol. 64, no. 4, pp. 1263–1278, 2015.
- [3] C. Studer, S. Medjkouh, E. Gonultaş, T. Goldstein, and O. Tirkkonen, “Channel charting: Locating users within the radio environment using channel state information,” *IEEE Access*, vol. 6, no. 3, pp. 47 682–47 698, 2018.
- [4] M. Stahlke, G. Yammine, T. Feigl, B. M. Eskofier, and C. Mutschler, “Velocity-based channel charting with spatial distribution map matching,” *IEEE J. of Indoor and Seamless Positioning and Navigation*, vol. 2, no. 1, pp. 230–239, 2024.
- [5] P. Ferrand, A. Decurninge, L. G. Ordoñez, and M. Guillaud, “Triplet-based wireless channel charting,” in *IEEE Global Comms. Conf.*, Taipei, Taiwan, 2020, pp. 1–6.
- [6] P. Stephan, F. Euchner, and S. Ten Brink, “Angle-delay profile-based and timestamp-aided dissimilarity metrics for channel charting,” *IEEE Trans. on Comms.*, vol. 72, no. 9, pp. 5611–5625, 2024.
- [7] J. Fontaine, B. Van Herbruggen, A. Shahid, S. Kram, M. Stahlke, and E. De Poorter, “Ultra wideband (uwb) localization using active cir-based fingerprinting,” *IEEE Comms. Letters*, vol. 27, no. 5, pp. 1322–1326, 2023.
- [8] R. Poeggel et al., “Passive Channel Charting: Locating Passive Targets using a UWB Mesh,” in *Proc. Intl. Conf. on Indoor Positioning and Indoor Navigation (IPIN)*, Tampere, FIN, 2025, pp. 1–6.
- [9] J. Wu, Y. Zhang, M. Zukerman, and E. K.-N. Yung, “Energy-efficient base-stations sleep-mode techniques in green cellular networks: A survey,” *IEEE Comms. Surveys & Tutorials*, vol. 17, no. 2, pp. 803–826, 2015.
- [10] T. Bai, R. Vaze, and R. W. Heath, “Analysis of blockage effects on urban cellular networks,” *IEEE Trans. on Wireless Comms.*, vol. 13, no. 9, pp. 5070–5083, 2014.
- [11] J. Lorincz, L. Chiaravaglio, and F. Cuomo, “A measurement study of short-time cell outages in mobile cellular networks,” *Computer Comms.*, vol. 79, no. 1, pp. 92–102, 2016.
- [12] A. Vaswani et al., “Attention is all you need,” in *Advances in Neural Information Processing Systems*, Long Beach, CA, 2017, pp. 5998–6008.
- [13] J. Deng, S. Medjkouh, N. Malm, O. Tirkkonen, and C. Studer, “Multipoint channel charting for wireless networks,” in *IEEE Proc. Intl. Conf. on Signals, Systems, and Computers (Asilomar)*, Pacific Grove, CA, 2018, pp. 286–290.
- [14] L. Le Magoarou, “Efficient channel charting via phase-insensitive distance computation,” *IEEE Wireless Comms. Letters*, vol. 10, no. 12, pp. 2634–2638, 2021.
- [15] M. Stahlke, G. Yammine, T. Feigl, B. Eskofier, and C. Mutschler, “Indoor localization with robust global channel charting: A time-distance-based approach,” *IEEE Trans. on Machine Learning in Comms. and Networking*, vol. 1, no. 1, pp. 3–17, 2023.
- [16] E. Lei, O. Castañeda, O. Tirkkonen, T. Goldstein, and C. Studer, “Siamese neural networks for wireless positioning and channel charting,” in *Proc. Intl. Conf. on Comm., Control, and Computing (Allerton)*, Piscataway, NJ, 2019, pp. 200–207.
- [17] M. Stahlke, G. Yammine, T. Feigl, B. M. Eskofier, and C. Mutschler, “Velocity-based channel charting with spatial distribution map matching,” *IEEE J. of Indoor and Seamless Positioning and Navigation*, vol. 2, no. 1, 2024.
- [18] E. Hoffer and N. Ailon, “Deep metric learning using triplet network,” in *Similarity-Based Pattern Recognition*, Copenhagen, Denmark, 2015, pp. 84–92.
- [19] G. Koch, R. Zemel, R. Salakhutdinov, et al., “Siamese neural networks for one-shot image recognition,” in *ICML deep learning workshop*, vol. 2, Lille, France, 2015, pp. 1–30.
- [20] I. Loshchilov and F. Hutter, “Decoupled weight decay regularization,” *arXiv:1711.05101 [cs.LG]*, pp. 1–19, 2019.
- [21] F. Euchner and M. Gauger, *CSI Dataset dichasus-cf0x: Distributed Antenna Setup in Industrial Environment*, <https://doi.org/doi:10.18419/darus-2854>, Accessed: 10.07.2025, 2022.
- [22] F. I. for Integrated Circuits IIS, *Fingerprinting dataset for positioning: 5g dataset*, <https://www.iis.fraunhofer.de/en/ff/lv/dataanalytics/pos/fingerprinting-dataset-for-positioning.html>, Accessed: 28.07.2025, 2023.
- [23] A. Salihu, M. Rupp, and S. Schwarz, “Self-supervised and invariant representations for wireless localization,” *IEEE Trans. on Wireless Comms.*, vol. 23, no. 8, pp. 8281–8296, 2024.